LAND DEGRADATION & DEVELOPMENT
Land Degrad. Develop. **26**: 158–167 (2015)
Published online 26 December 2012 in Wiley Online Library (wileyonlinelibrary.com) **DOI**: 10.1002/ldr.2193

OBJECT-BASED MAPPING OF KARST ROCKY DESERTIFICATION USING A SUPPORT VECTOR MACHINE

E.-Q. XU[1,2], H.-Q. ZHANG[1]* AND M.-X. LI[3]

[1]*Institute of Geographic Sciences and Natural Resources Research, Chinese Academy of Sciences, Beijing 100101, PR China*
[2]*Graduate University, Chinese Academy of Sciences, Beijing 100049, PR China*
[3]*Combating Desertification Management Center of State Forestry Administration, Beijing 100714, PR China*

Received: 10 August 2012; Revised: 5 September 2012; Accepted: 14 November 2012

ABSTRACT

Accurate and cost-effective mapping of karst rocky desertification (KRD) is still a challenge at the regional and national scale. Visual interpretation has been utilised in the majority of studies, while an automated method based on pixel data has been investigated repeatedly. An object-based method coupling with support vector machine (SVM) was developed and tested using Enhanced Thematic Mapper Plus (ETM+) images from three selected counties (Liujiang, Changshun and Zhenyuan) with different karst landscapes in SW China. The method supports a strategy of defining a mapping unit. It combined ETM+ images and ancillary data including elevation, slope and Normalized Difference Vegetation Index images. A sequence of scale parameters estimation, image segmentation, training data sampling, SVM parameters tuning and object classification was performed to achieve the mapping. A quantitative and semi-automated approach was used to estimate scale parameters for segmenting an object at an optimal scale. We calculated the sum of area-weighted standard deviation (*WS*), rate of change for *WS*, local variance (*LV*) and rate of change for *LV* at each scale level, and the threshold of the aforementioned index that indicated the optimal segment level and merge level. The KRD classification results had overall accuracies of 85·50, 84·00 and 84·86 per cent for Liujiang, Changshun and Zhenyuan, respectively, and kappa coefficients are up to 0·8062, 0·7917 and 0·8083, respectively. This approach mapped six classes of KRD and offered a visually appealing presentation. Moreover, it proposed a conceptual and size-variable object from the classification standard of KRD. The results demonstrate that the application of our method provides an efficient approach for the mapping of KRD. Copyright © 2012 John Wiley & Sons, Ltd.

KEY WORDS: karst rocky desertification; object-based; image segmentation; optimal object scale; different karst landscapes; China

INTRODUCTION

The karst region in southwestern China is about 540,000 km^2 including eight provinces, which lie at the heart of the eastern Asia area, and form one of world's three foremost karst centres. This unique geomorphological feature, characterised by contiguous distribution of bare carbonate, makes it an ecologically fragile area in the context of climate change (Sweeting, 1995). Karst rocky desertification (KRD) has been identified as the most severe environmental degradation that threatens southwest China (Wang, 2002; Wang *et al*., 2004; Bai *et al*., in press). Negative environmental impacts include loss of cultivated soil, water shortage, soil erosion and decreased biodiversity. Meanwhile, the social and economic well-being of the people in the region have also been jeopardised (Wang *et al*., 2004). The deterioration of the environment in the southwestern karst region has become a cause for concern at the highest levels for the Chinese Government. The National Reform and Development Commission has started the implementation of a 3-year pilot project to control and restore KRD in 100 counties of karst region. To this end, studies that accurately portray the location, quality and quantity of the KRD area in this region are urgently needed to serve as a basis for understanding the current KRD status as well as developing sustainable restoration practice.

Remote sensing technology has been the favoured type of approach for mapping KRD (Zhou, 2001; Chen *et al*., 2007; Huang and Cai, 2007; Liu *et al*., 2008; Li *et al*., 2009; Bai *et al*., in press), thanks to its spatial explicit and temporal dynamic attributes. Early work with satellite imagery for local-scale KRD mapping relied on visual interpretation. It utilised colour-related features and structural elements such as size, pattern, configuration and association to recognise surface features (Campbell, 2002). Also, the interpreter tells signal from noise, in other words, distinguishing information against a 'simplified' environment through human perception (Bruce *et al*., 2003). Because the human brain and expertise are the best image processors, visual interpretation by analysts shows high accuracy in mapping rocky desertification.

Although visual interpretation of satellite images is commonly used for identifying KRD, more recent work has emphasised digital image classification, primarily because the analysis is many times faster. Meanwhile, subjectivity might be involved in visual interpretation and thus increases the risk of omissions. To overcome these limitations, automated image classification methods including supervised method, machine learning algorithm, rock-desertification

*Correspondence to: H.-Q. Zhang, Institute of Geographic Sciences and Natural Resources Research, Chinese Academy of Sciences, Beijing 100101, PR China.
E-mail: zhanghq@igsnrr.ac.cn

index and spectral unmixing model have been extensively applied in mapping KRD. Huang and Cai (2009) used supervised maximum likelihood classification with different input bands to map karst rock. Chen *et al.* (2003) built a rock-desertification extraction model on the basis of spectral characteristics of different rock-desertification classes. Yu (2009) applied CART decision tree to extract rocky desertification. Yan *et al.* (2009) classified rocky desertification on the basis of neural network classification and spectrum. The NDVI (Zhang *et al.*, 2008) and band5/band4 (Tong, 2003) of TM imagery were calculated to identify rocky desertification. Xia *et al.* (2006) introduced a definition of vegetation line and the Geometrical Rock-desertification Index with spectral unmixing model to map rocky desertification. Yue *et al.* (2008) used the spectral unmixing model on the basis of the Monte Carlo approach to extract KRD information with EO-1 Hyperion®. Yue *et al.* (2011) developed a KRD synthesis index for the unique spectral features to observe non-vegetation land cover types.

The automatic methods mentioned earlier are based on the pixel and extract useful information from individual pixels, which are substantively inhibited by contributions of signals from surrounding pixels. Many researchers have claimed that pixel-based classification has a relatively low accuracy in terms of classification results (Muller *et al.*, 1993; Ivits *et al.*, 2005; Yu *et al.*, 2006; Van de Voorde *et al.*, 2007). This is particularly true in karst areas, where the pixel-based classification method shows lower classification accuracy because of larger terrain difference and more broken surface block (Tong, 2003). It is suggested that surrounding pixels should be taken into consideration for automatic classification.

On the other hand, object-based method provides an innovative way for analysing digital imagery (Blaschke, 2010). Whereas pixel-based image analysis is based on the information in each pixel, object-based image analysis (OBIA) is based on information from a set of similar pixels called objects or image objects. More specifically, image objects are groups of pixels that are similar to one another based on a measure of spectral properties (i.e., colour, size, shape and texture), as well as context from a neighbourhood surrounding the pixels (Tormos *et al.*, 2012). Because of this feature, object-based processing techniques are becoming more popular compared with traditional pixel-based image analysis when information of surrounding pixels is needed for classification (Gamanya *et al.*, 2009; Blaschke, 2010). Many studies comparing OBIA and pixel-based classification approaches revealed a higher accuracy result with object-based method (Willhauck *et al.*, 2000; Yan *et al.*, 2006; Myint *et al.*, 2011; Whiteside *et al.*, 2011). See Blaschke (2010) for a detailed discussion on the object-based method. The application of OBIA in mapping rocky desertification, however, has been limited. Xiong *et al.* (2008) started to use the object-based method to extract outlines of rocky desertification areas but just manually classified different KRD levels.

Another limitation of current digital mapping lies in the scale issues, which is not very clear in previous studies. The vegetation/soil cover and bedrock exposure are basically the classification criteria for the rocky desertification degree. The preceding criteria should be calculated in the given units. In other words, the KRD mapping is performed in a specific scale. But there is no consistent rule for defining the scale of mapping unit to compute the aforementioned rocky desertification characteristics. Hu *et al.* (2010) emphasised the consideration of the scale in the classification standard of KRD. The area of units was different in different studies (Tong, 2003; Li *et al.*, 2009; Chen and Wang, 2010). Li *et al.* (2010) indicated differences among assessment results with different grids.

The object-based method can be used as the mapping unit defining strategy. The object of KRD is to present a conceptual object such as burned areas (Mitri and Gitas, 2004) or tornado damaged areas (Myint *et al.*, 2008) in other object-based methods using multi-spectral images. The concept is from the classification standard of KRD. The conceptual object of KRD is a mixture of different surface features with similar vegetation/soil cover and bedrock exposure. But can the object-based method using mid-resolution image fulfil the required accuracy?

The objective of this study was to develop a cost-effective and time-saving mapping technique with an objective mapping unit defining strategy, which could take scale issues into consideration. We will investigate the applicability and performance of our method for mapping KRD with Enhanced Thematic Mapper Plus (ETM+) images coupled with ancillary data.

STUDY AREA AND DATA

Study Area

The three selected sites represent different KRD landscapes with different proportion of KRD classes. More explanation about the class types of KRD are presented in the Methods section. Also the three sites have a marked diversity of environmental and social characteristics, such as geology, topography and climate. Liujiang County is located in Guangxi Province, and the other two counties are in Guizhou Province (Figure 1). Details are as follows.

Site 1: Liujiang County

This county is dominated by karst hill landscape, where relief amplitude is small and the relative elevation is usually between 100 and 150 m. The total area is 2539 km^2 with elevation ranging from 37 to 664 m. The terrain slopes from east and southwest to the centre. Karst areas cover about 97 per cent of the county. Two major KRD types in this area are light KRD and moderate KRD.

Site 2: Changshun County

This county covers an area of 1552 km^2 within karst peak-cluster depression landscape, which contains a combination of karst cones and depressions between cones. Its elevation is between 661 and 1572 m. More than 97 per cent of the land is karst area. The proportion of

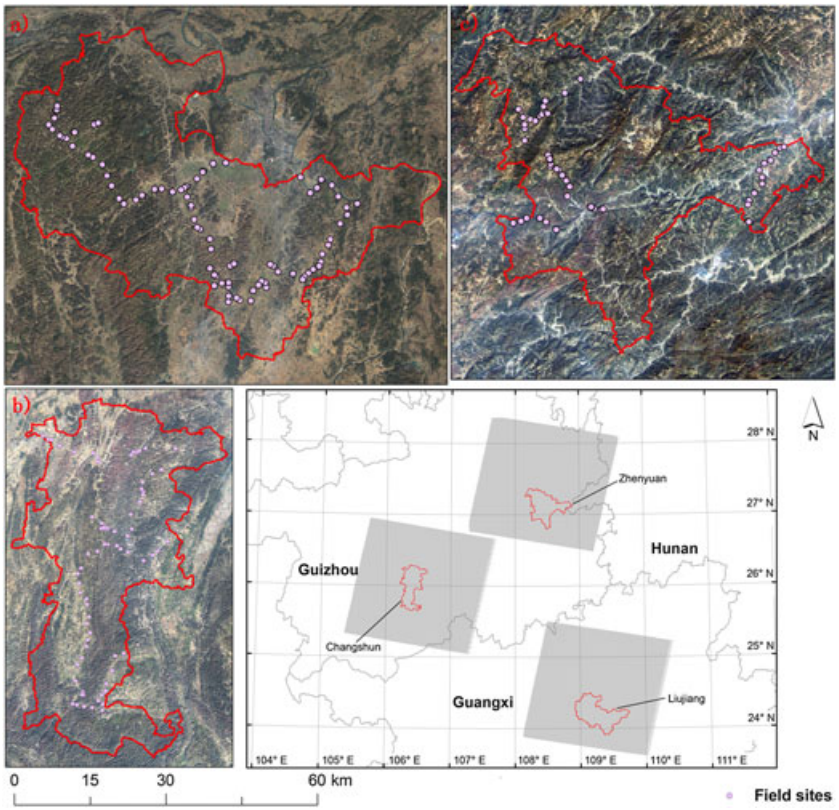

Figure 1. The location of study sites in (a) Liujiang, (b) Changshun and (c) Zhenyuan. This figure is available in colour online at wileyonlinelibrary.com/journal/ldr.

KRD in the county is up to 30 per cent. Among the three, Changshun County suffers the most serious KRD, making it one of the most KRD affected counties in Guizhou (Wang, 2010).

Site 3: Zhenyuan County

The total area of Zhenyuan County is 1880 km^2 with a karst trough valley landscape, where the valley is formed by karst erosion. The elevation ranges from 287 to 1301 m. Only 45 per cent of the land is karst area. The KRD areas cluster together. Severe KRD is the largest class of KRD recorded for the county and it especially common in the west.

Satellite Data and Preprocessing

The ETM+ imaging was chosen because it has a relatively wide coverage and a short repeat cycle, which are suitable to mapping KRD at a regional scale. The images used are strip-repaired ETM+ images, which are provided by the International Scientific Data Service Platform, Computer Network Information Center, Chinese Academy of Sciences (http://datamirror.csdb.cn). Six spectral bands in the visible, near-infrared and shortwave infrared at 30-m nominal pixel size were used in this study. Table I presents details of paths, rows and acquisition dates for each county.

Preprocessing included geometric correction and atmosphere correction. Geometric correction incorporates the digital elevation model (DEM) with 30 ground control points taken from a 1:50,000 topographic map (provided by the Institute of Geographic Sciences and Natural Resources Research, Chinese Academy of Sciences) producing a root-mean-square error of less than 0·5 pixel for each image. The FLAASH module in the Environment for Visualizing Images (ENVI)® software (ITT Visual Information Solutions, 2009) was used for atmosphere correction.

Ancillary Datasets

The elevation and slope were taken into account for this study, because topographical factors would influence the KRD distribution (Huang and Cai, 2007). The Normalized Difference Vegetation Index (NDVI) image was chosen because of the vegetation cover as one standard of the KRD. The elevation images are provided by the International Scientific Data Service Platform, Computer Network Information Center, Chinese Academy of Sciences (http://datamirror.csdb.cn). A slope image (degree) was generated by the DEM image. The six spectral bands, vegetation index image and topographic index images were combined to

Table I. Landsat image description

County	Path	Row	Date
Liujiang	125	43	2/11/2010
Changshun	127	42	31/10/2010
Zhenyuan	126	41	9/11/2010

Table II. Image layers used in object-based classifications

Spectral bands	Vegetation index	Topographic index
Band 1 Blue	NDVI	Elevation
Band 2 Green		Slope (degrees)
Band 3 Red		
Band 4 Near infrared		
Band 5 Shortwave infrared		
Band 7 Shortwave infrared		

a data set consisting of nine individual layers (Table II). The six spectral bands were used as input data to the image segmentation processing, and all the layers were used for classification of the KRD.

METHODS

Categorising Framework of Karst Rocky Desertification

Non-karst areas were ruled out for mapping the KRD on the basis of the lithology distribution map, and karst areas were classified no KRD, potential KRD and KRD with four types (slight, moderate, severe and extremely severe) as shown in Table III. This classification standard was based on the bedrock exposure and the coverage of vegetation plus soil within mapping unit (Li *et al*., 2009). The KRD classes are the focus in a related study; four types of KRD within the field are shown in Figure 2.

A total of nine classes were identified in the support vector machine (SVM) classification. This is because no KRD areas include four classes with significantly different object features. The four classes are built-up area, water, bare soil (mainly harvested farmlands) and high vegetation cover surface. After the classification, we grouped the aforementioned four classes into no KRD to map the final KRD result.

Image Segmentation and Object Feature Selection

Image segmentation was a crucial step in object-based classification. Numerous image segmentation algorithms were developed and assessed (Neubert and Herold, 2008; Neubert *et al*., 2008). The segmentation was performed by the ENVI Feature Extraction Module version 4.6 (ITT Visual Information Solutions, 2008) in this study. It involved two processes: (i) segment the image and (ii) merge the image. The two scale parameters were segment level and merge level with a range from 0 to 100. The larger the two scale parameters were, the coarser the object was. We should ensure that the segment was not over-segmented or under-segmented. Therefore, we plotted some index against the image segment and merge level with one step size. Finally, we estimated the scale parameter for an optimal object size from the curve.

The first process should ensure that features of interest were not grouped into segments represented by other features, so we took homogeneity of each object into consideration to identify the segment level. The homogeneity was defined as sum of area-weighted standard deviation (*WS*) of each object for each segment level. We chose the segment level when the *WS* curve started steepening.

$$WS = \frac{\sum_{i=1}^{N}(a_i * s_i)}{\sum_{i=1}^{N} a_i}$$

Where: N is number of objects; a_i is area of each object; s_i is standard deviation of each object value.

To assess the dynamics of *WS*, we used a measure called rate of change for *WS* (*ROC-WS*).

$$ROC\text{-}WS = \frac{WS - (WS - 1)}{WS - 1}$$

Where: WS is the *WS* at target level and $WS - 1$ is the *WS* at the next lower level.

If objects are formed by similar features, the *ROC-WS* has a stable growth with increasing segmentation level. Until objects are grouped into segments that are represented by other features, the homogeneity of objects decreases significantly. We hypothesised that a significant increase in *ROC-WS* plot indicated that the object was under-segmented and the segmentation should be stopped.

The second process was a refined procedure. The relatively homogeneous objects were merged into a larger variance in the total image. Kim *et al*. (2008) estimated the optimal object size by making advances of local variance (*LV*). *LV* was defined as the mean standard deviation of the objects through segmentation to explore the heterogeneity of all the objects for each scale level.

$$LV = \sqrt{\frac{1}{N-1}\sum_{i=1}^{N}(m - \overline{m})^2}$$

Where: m is the mean of each object value and $\bar{m}$ indicates all objects' mean.

Table III. Classification standard of karst rocky desertification

	Bedrock exposure (%)	Vegetation and soil cover (%)
No karst rocky desertification (no KRD)	<20	>80
Potential karst rocky desertification (potential KRD)	20–30	70–80
Light karst rocky desertification (light KRD)	31–50	50–69
Moderate karst rocky desertification (moderate KRD)	51–70	30–49
Severe karst rocky desertification (severe KRD)	71–90	10–29
Extremely severe karst rocky desertification (extremely severe KRD)	>90	<10

Figure 2. Karst rocky desertification: (a) extremely severe, (b) severe, (c) moderate and (d) light. This figure is available in colour online at wileyonlinelibrary.com/journal/ldr.

The optimal segmentation would actually occur at the scale just before the levelling off of the graph. Drăguţ *et al*. (2010) used the *ROC-LV* to assess the dynamics of *LV*; the peaks of *ROC-LV* indicated that the image could be segmented in the most appropriate manner.

$$ROC\text{-}LV = \frac{LV - (LV - 1)}{LV - 1}$$

Where: LV is the *LV* at target level and $LV - 1$ is the *LV* at the next lower level.

The mean of six spectral bands reflectance was used for the calculation of *WS*, *ROC-WS*, *LV* and *ROC-LV*. Thus we segmented the image at the optimal scale. In the next step, the Feature Extraction Module calculated the object features including spectral, textural and spatial features (ITT Visual Information Solutions, 2008). We chose only spectral and textural features for the next classification (Table IV).

Support Vector Machine

As one of the modern and robust supervised machine learning algorithms, the SVM can better solve the problem of small training set sizes, which is a popular machine learning algorithm for classification (Chang and Lin, 2011). In this work, we used the LIBSVM® package (Chang and Lin, 2011) for supervised classification and its extension LIBSVM-farutoUltimate® Version for tuning of LIBSVM parameters (software available at http://www.ilovematlab.cn) in the MATLAB® program environment. The kernel function used in this work was the radial basis function (RBF) kernel. We chose the C-SVC for mapping KRD. Overall classification accuracy has been influenced by the parameters used in the SVM (Burges, 1998). The two tuning parameters using the RBF kernel for LIBSVM are 'cost' (C) and 'sigma' (σ). A larger C corresponds to assigning a higher penalty to errors (Burges, 1998), and the σ affected the shape of the separating hyperplane (Huang *et al*., 2002). The extension package tuned both of the parameters on the basis of the Grid Search algorithm.

Table IV. Object feature selection

Categories	Description	
Spectral features	MINBAND_x	Minimum value of the pixels comprising the object
	MAXBAND_x	Maximum value of the pixels comprising the object
	AVGBAND_x	Average value of the pixels comprising object
	STDBAND_x	Standard deviation value of the pixels comprising object
Textural features	TX_RANGE	Average data range of the pixels comprising the region inside the kernel (a kernel is an array of pixels used to constrain an operation to a subset of pixels)
	TX_MEAN	Average value of the pixels comprising the region inside the kernel
	TX_VARIANCE	Average variance of the pixels comprising the region inside the kernel
	TX_ENTROPY	Average entropy value of the pixels comprising the region inside the kernel. ENVI EX computes entropy, in part, from the Max Bins in Histogram preference

A repeated 20-fold cross-validation was used to create parameters on the basis of the training data set.

Sample Data and Accuracy Assessment

We chose objects of the segment as sampling units for training model and accuracy assessment. A training data set was required for machine learning and tuning parameters in the SVM classification. All training data were chosen representatively by simple random sampling from the segment image to create a training set. The training data set including all nine classes were about 5 per cent of the image, which were classified from visual interpretation. We collected 81, 86 and 54 field data for visual interpretation in Liujiang, Changshun and Zhenyuan, respectively. The field data were collected as the classification standard shown in Table III within an area of ~0·01 km^2.

The fitting degree of boundaries was not assessed, but we focused on assessing the classification accuracy. The testing data from visual interpretation were derived from a stratified random sampling over the classification results. The number of ground reference data of Liujiang, Changshun and Zhenyuan was 1000, 800 and 700, respectively.

Confusion matrices and kappa statistics were used for accuracy assessment (Congalton, 1991). A confusion matrix provided the overall accuracy (OA) (i.e. the percentage of correctly classified types), the producer's accuracy (*PA*) and the user's accuracy (*UA*). The *PA* means the probability that a classified type actually represents that category in reality; and the *UA* indicates the probability that a classified type represents for which it has been assigned (Congalton and Green, 2009). The kappa coefficients and conditional kappa (*CK*) were also calculated.

RESULTS

Segment Results

In three sites, the curve of *WS*, *ROC-WS*, *LV* and *ROC-LV* yielded similar variation trends (Figure 3). Variations of

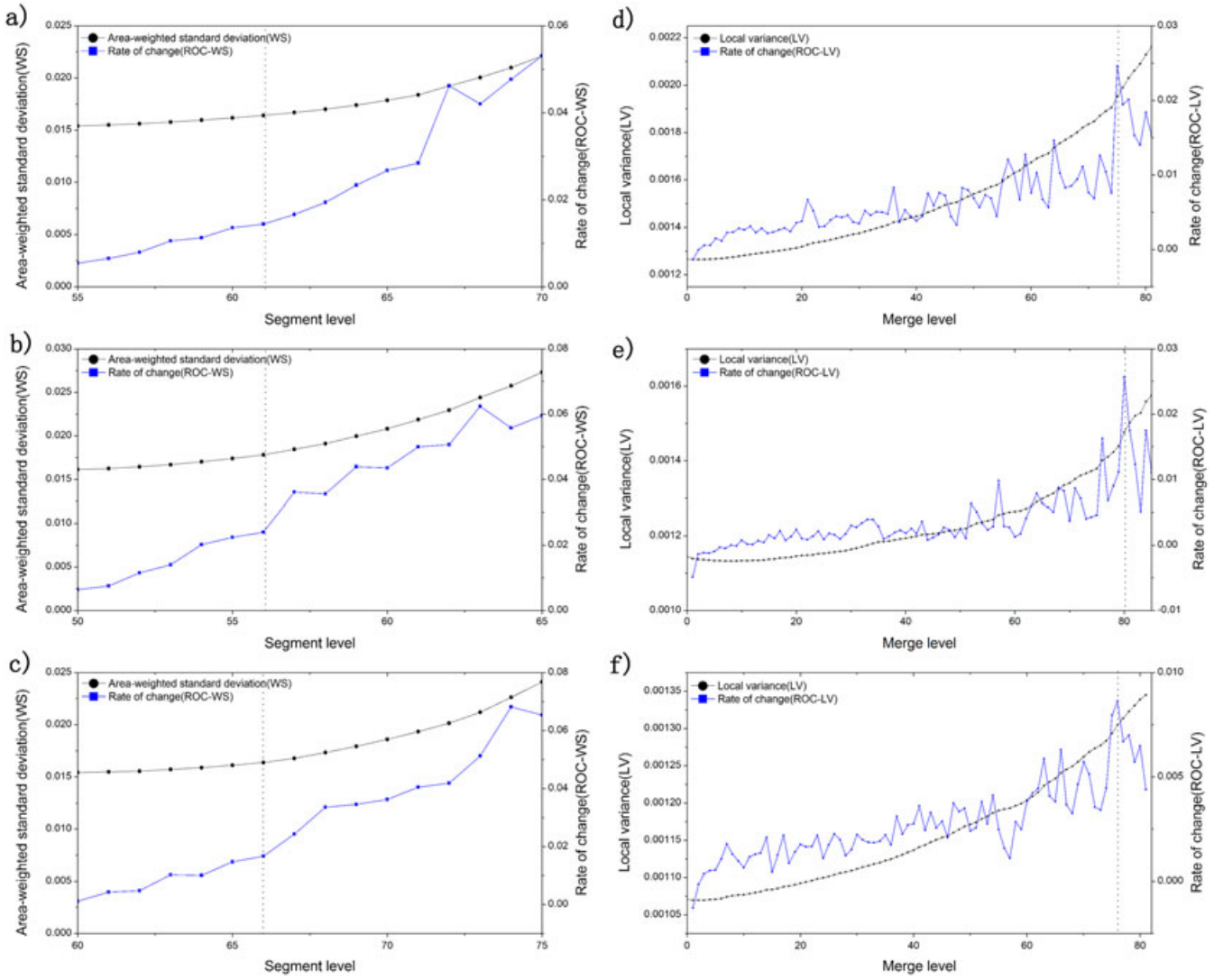

Figure 3. *WS* and *ROC-WS* as a function of the segment level in (a) Liujiang, (b) Changshun and (c) Zhenyuan; *LV* and *ROC-LV* as a function of the merge level in (d) Liujiang, (e) Changshun and (f) Zhenyuan. This figure is available in colour online at wileyonlinelibrary.com/journal/ldr.

WS and *ROC-WS* were fuzzy in the fine segment level because the *WS* stayed stable. The *WS* increased with the segment level, and the *ROC-WS* increased as well. The *ROC-WS* enhanced the visualisation of *WS* changing trend. We defined the threshold as the pint at which *WS* curve obviously started to steepen forming a first break arose in the *ROC-WS* curve. In our study, the segment level of Liujiang, Changshun and Zhenyuan were 61, 56 and 66, respectively (Figure 3a–c).

The *LV* decreased at a very fine scale and increased quickly as the merge level increased, whereas the *ROC-LV* showed an upward fluctuating trend. The peak means that segments correspond to ground truth, but also it is induced by the segment image background (i.e. complex classes landscape) (Drăguţ *et al*., 2010). Therefore, it showed several peaks in the *ROC-LV*. In any case, we set the threshold as the obvious break in *ROC-LV* curve whereas the *LV* curve levelled off relatively. Because the homogeneity reduced quickly in a very coarse scale, we obscured the curve on a coarse scale. Finally, the merge level of Liujiang, Changshun and Zhenyuan was identified as 75, 80 and 76, respectively (Figure 3d–f).

With the aforementioned scale parameters, we performed two steps for segmenting and merging images to produce the optimal size objects. Portions of image segmentation results are shown in Figure 4, which shows that objects within the segmentation follow the spectral boundaries closely.

Accuracy Assessment

The classification results are shown in Figure 5. The no KRD category dominated the majority of the area of three sites. The potential, slight and moderate KRD cover larger sizes, compared with severe and extremely severe KRD, which is scattered in the three counties. One exception is that KRD in Zhenyuan covers a considerable area.

Although there were biases in visual interpretation, the total accuracy assessment results can be reliable because visual interpretation has been used in most KRD studies. A summary of the accuracy assessment of the object-based classifications for three sites is presented. OAs of Liujiang, Changshun and Zhenyuan are 85·50, 84·00 and 84·86 per cent, respectively. Meanwhile, kappa coefficients are 0·8062, 0·7917 and 0·8083 (Figure 6). Although three sites represent three different karst landscapes, the assessment results were similar at last. The accuracy assessment of Changshun is a little poor by contrast. All these indicate that our method is suitable for mapping KRD within different karst landscapes on the whole. The *CK* of severe KRD in Zhenyuan especially provided a significantly higher accuracy of 0·83 than the other two. For other different types of KRD, the assessment result within the same type of KRD for three sites does not have a significant difference (Table V).

The *PA*s, *UA*s and *CK*s for each class are shown in Table V. For different classes, a better performance is achieved in the classes with a larger area. The accuracy assessments of no KRD are the highest (*CK*s are 0·93, 0·87 and 0·91 for Liujiang, Changshun and Zhenyuan; and *UA*s are 96·32, 92·16 and 94·34 per cent, respectively). Less accurate results are observed from the potential KRD and light KRD with *PA*s and *UA*s of about 80 per cent. *CK*s are 0·78, 0·76 and 0·82 for potential KRD in threes sites, and *CK*s of light KRD are 0·82, 0·80 and 0·77, respectively. The classifications of moderate KRD, severe KRD and extremely severe KRD have the lowest accuracy (*CK*s range from 0·70 to 0·76) except for the severe KRD in Zhenyuan because of its cluster distribution. In addition, all the *PA*s of extremely severe KRD in three sites are 100 per cent whereas the *PA*s are 72·22, 72·97 and 73·68 per cent, respectively. The gaps between *PA*s and *UA*s of moderate KRD and severe KRD showed a similar characteristic. However, the gap between *PA*s and *UA*s of no KRD in Liujiang and Zhenyuan has an opposite characteristic. In any case, it indicates that the object-based classification with SVM is accurate and effective for mapping KRD.

DISCUSSION

There have been numerous attempts at mapping KRD using high-resolution or multi-spectral images. Because of large terrain differences and broken surfaces, it is still a challenge to achieve a better accuracy. In the pixel or sub-pixel mapping method, the pixel is the mapping target of interest (Tong, 2003; Xia *et al*., 2006; Yue *et al*., 2008; Yan *et al*., 2009; Yu, 2009), rather than actual image objects. In contrast, the object-based method mapping the actual image objects

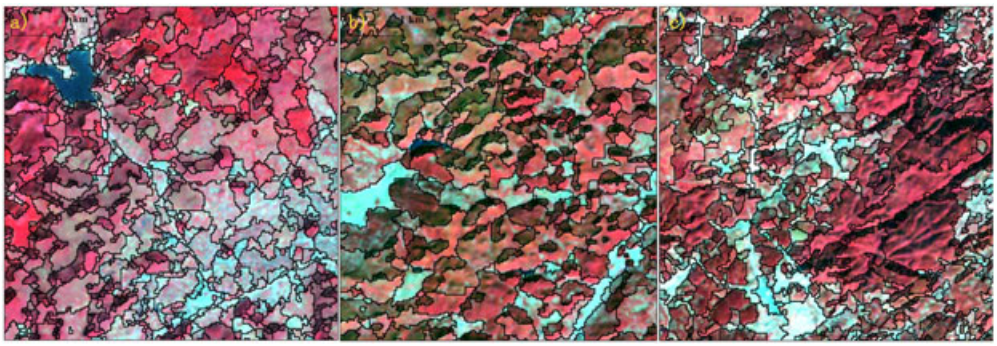

Figure 4. A section of segment result in (a) Liujiang, (b) Changshun and (c) Zhenyuan. This figure is available in colour online at wileyonlinelibrary.com/journal/ldr.

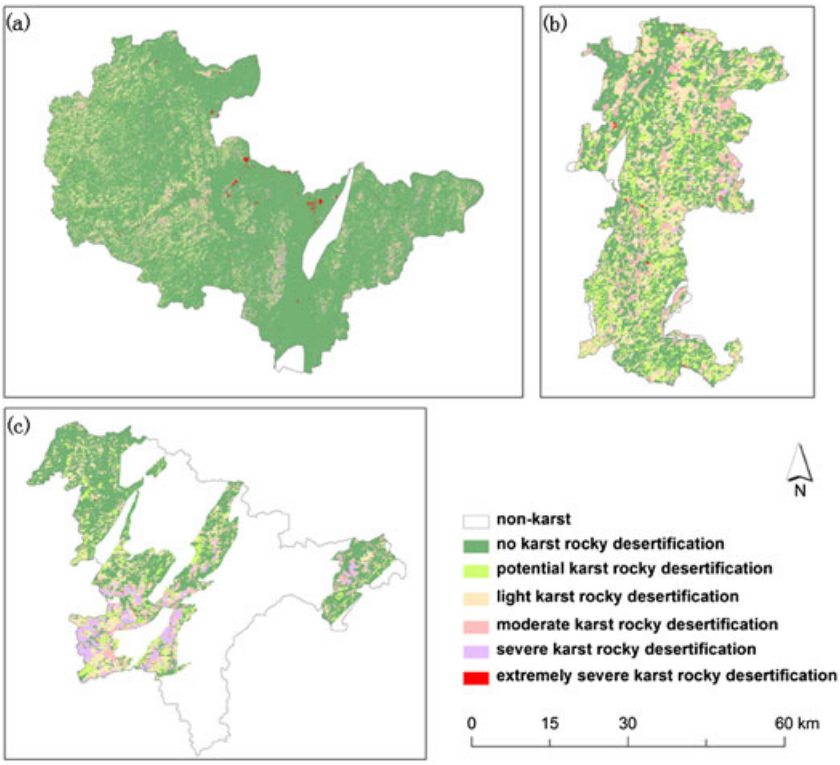

Figure 5. Results of object-based classification for karst rocky desertification using SVM in a) Liujiang, b) Changshun, c) Zhenyuan. This figure is available in colour online at wileyonlinelibrary.com/journal/ldr.

offered a more generalised visual appearance such as the manual interpretation (Stuckens *et al*., 2000).

For the mapping effect, merging pixels (Tong, 2003; Chen and Wang, 2010) or filter by sliding windows (Yu, 2009) are required in the pixel-based method. To a certain extent, the mapping unit is chosen subjectively and arbitrarily. As a result, it easily includes uncertainties. However, our approach mapped KRD in objects which are derived without subjectivity. Through a quantitative estimation of an optimal scale, we performed the segmentation for forming objects. An object is a variable unit with the expectation that it will divide the image into (i) relatively homogeneous and (ii) statistically significant groups of pixels (Blaschke, 2010).

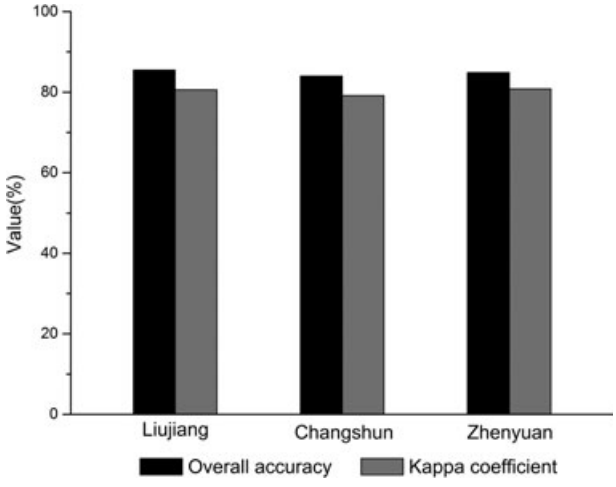

Figure 6. Overall accuracies and kappa coefficients for the three sites.

The errors in mapping KRD mainly resulted from confusion between classes because of their similar spectral behaviour. From the KRD classification standard, the KRD classes were an ordinal classification series with a gradient of the bedrock exposure and the coverage of vegetation plus soil. Thus it was easily confused when the KRD classification feature of the object is in the threshold of two adjacent classes except for no KRD and extremely severe KRD. For no KRD and extremely severe KRD, separating them from adjacent classes was much easier because of the relative pureness with vegetation/soil and bedrock, respectively.

Furthermore, the spectral responses of karst rock and built-up areas are very similar, so it was challenging to separate these two categories (Huang and Cai, 2009). A similar situation happened between the tiny areas with bare soil and severe KRD or extremely severe KRD areas. Under the circumstances, the ancillary data could be a big help to assist in the classification. For example, the variations of elevation in objects were calculated for classification. Thus the built-up area and soil with relatively consistent elevation and low slope can be distinguished from the karst rock with variable elevations in an object. This variation feature cannot be reflected in a pixel. Therefore, it is an advantage for the object-based classification compared with the pixel-based method.

But tiny plots of harvested sloping farmland can still be confused with severe KRD or extremely severe KRD areas.

Table V. Accuracy of object-based classifications including the *PA*, *UA* and *CK* for each class

	Liujiang			Changshun			Zhenyuan		
	PA (%)	*UA* (%)	*CK*	*PA* (%)	*UA* (%)	*CK*	*PA* (%)	*UA* (%)	*CK*
No KRD	82·25	96·32	0·93	87·85	92·16	0·87	79·05	94·34	0·91
Potential KRD	91·89	81·73	0·78	80·00	80·00	0·76	82·11	84·78	0·82
Light KRD	71·88	84·56	0·82	75·00	83·48	0·80	80·16	81·45	0·77
Moderate KRD	97·22	72·92	0·70	76·70	79·00	0·76	93·86	76·43	0·72
Severe KRD	95·24	76·92	0·75	88·41	76·25	0·74	95·24	85·11	0·83
Extremely severe KRD	100·0	72·22	0·71	100·0	72·97	0·71	100·0	73·68	0·73

PA, producer's accuracy; UA, user's accuracy; CK, conditional kappa.

Confusion even occurs in some moderate KRD areas. As a result, moderate KRD, severe KRD and especially extremely severe KRD have been slightly overestimated from no KRD, which are reflected in the gap between *PA* and *UA* for the aforementioned classes. In addition, over-segment or under-segment induced errors as well.

Moreover, the limited shadows in our study sites with high relief were not classified directly because of lacking effective topographic correction. In our study, training and testing data for shadow objects were classified by the NDVI index and the surrounding classes. However, the limited misclassified shadows do not have much effect on KRD categories. This should be investigated in future studies.

To improve the classification result, the existing geographic information system (GIS) thematic map coupled with object-based classification may give a higher accuracy (Durieux *et al*., 2008; Tormos *et al*., 2012). For example, the synchronous land use map can be used to extract tiny harvested sloping farmland from karst rock. Another idea is to optimise the segmentation process, which at present is only based on spectral information. With ancillary data, it may reduce the risks of over-segmentation and under-segmentation. It would be interesting in the near future to use more ancillary data, which influence the KRD, to optimize our classification.

CONCLUSIONS

An accurate and quick method for mapping KRD is required for a variety of implications at a regional scale. An object-based method with SVM was used for the aforementioned need in three typical karst sites. We integrated ETM+ images and ancillary data, and used a number of spectral and textural features for classification. The method provided a strategy of defining mapping unit. We estimated the two scale parameters for image segment, and mapped KRD in conceptual objects at an optimal scale. Compared with pixel-based method, it is an advantage for object-based classification to calculate the features within objects for better result. With better visual effects and the consideration of scale, it provided a quick and cost-effective way for mapping KRD. Our approach can fulfil the accuracy requirement for three sites with different landscapes. There are some limitations in our method, which need to be improved in the future works. Tiny harvested sloping farmland especially was still confused with the KRD areas; also the limited shadows were not effectively processing. Considering aforementioned limitations, suggestions include combination with auxiliary GIS data and optimisation of the segmentation process. The improvement mentioned earlier should be investigated in the future works.

ACKNOWLEDGEMENTS

This work was jointly supported by the National Program of Monitoring Desertification sponsored by Combating Desertification Management Center of State Forestry Administration of the People's Republic of China, and Program of Regional Sustainable Land Use sponsored by Ministry of Land and Resources of the People's Republic of China.

REFERENCES

Bai XY, Wang SJ, Xiong KN. in press. Assessing spatial–temporal evolution processes of karst rocky desertification land: indications for restoration strategies. *Land Degradation & Development*. DOI: 10.1002/ldr.1102.

Blaschke T. 2010. Object based image analysis for remote sensing. *ISPRS Journal of Photogrammetry and Remote Sensing* **65**: 2–16. DOI:10.1016/j.isprsjprs.2009.06.00.

Bruce V, Green PR, Georgeson MA. 2003. *Visual perception: physiology, psychology, & ecology* (4rd edn). Psychology Press: Hove & London.

Burges CJC. 1998. A tutorial on support vector machines for pattern recognition. *Data Mining and Knowledge Discovery* **2**: 121–167. DOI: 10.1023/A:1009715923555.

Campbell JB. 2002. *Introduction to remote sensing* (3rd edn). Guilford Press: New York, NY.

Chang CC, Lin CJ. 2011. LIBSVM: a library for support vector machines. *ACM Transactions on Intelligent Systems and Technology* **2**: 2721–2727. DOI:10.1145/1961189.1961199.

Chen HX, Wang JH. 2010. Investigation and research on karst rocky desertification area based on TM data. *Journal of Meteorological Research and Application* **31**: 41–43 (in Chinese with English abstract).

Chen QW, Lan AJ, Xiong KN, Xiao SZ, Wang J, Xiong J. 2003. Spectral feature-based model for extracting karst rock-desertification from remote sensing image. *Journal of Guizhou Normal University (Natural Sciences)* **21**: 82–87 (in Chinese with English abstract).

Chen QW, Xiong KN, Lan AJ. 2007. Analysis on karst rocky desertification in Guizhou based on "3S". *Carsologica Sinica* **26**: 37–42 (in Chinese with English abstract).

Congalton RG. 1991. A review of assessing the accuracy of classifications of remotely sensed data. *Remote Sensing of Environment* **37**: 35–46. DOI:10.1016/0034-4257(91)90048-B.

Congalton RG, Green K. 2009. *Assessing the accuracy of remotely sensed data: principles and practices*. CRC Press: Boca Raton, FL.

Drăguţ L, Tiede D, Levick SR. 2010. ESP: a tool to estimate scale parameter for multiresolution image segmentation of remotely sensed data.

International Journal of Geographical Information Science **24**: 859–871. DOI:10.1080/13658810903174803.

Durieux L, Lagabrielle E, Nelson A. 2008. A method for monitoring building construction in urban sprawl areas using object-based analysis of Spot 5 images and existing GIS data. *ISPRS Journal of Photogrammetry and Remote Sensing* **63**: 399–408. DOI:10.1016/j.isprsjprs.2008.01.00.

Gamanya R, De Maeyer P, De Dapper M. 2009. Object-oriented change detection for the city of Harare, Zimbabwe. *Expert Systems with Applications* **36**: 571–588. DOI:10.1016/j.eswa.2007.09.06.

Hu SG, Zhang ZX, Xia KJ. 2010. Information extraction of karst rocky desertification using remote sensing. *Journal of Geo-information Science* **12**: 870–879 (in Chinese with English abstract).

Huang C, Davis L, Townshend J. 2002. An assessment of support vector machines for land cover classification. *International Journal of Remote Sensing* **23**: 725–749. DOI:10.1080/01431160110040 323.

Huang QH, Cai YL. 2007. Spatial pattern of karst rock desertification in the Middle of Guizhou Province, Southwestern China. *Environmental Geology* **52**: 1325–1330. DOI: 10.1007/s00254-006- 0572-y.

Huang QH, Cai YL. 2009. Mapping karst rock in southwest China. *Mountain Research and Development* **29**: 14–20. DOI: 10.1659/mrd.857.

ITT Visual Information Solutions 2008. *ENVI feature extraction module user's guide*.

ITT Visual Information Solutions 2009. *Atmospheric correction module: QUAC and FLAASH user's guide*.

Ivits E, Koch B, Blaschke T, Jochum M, Adler P. 2005. Landscape structure assessment with image grey-values and object-based classification at three spatial resolutions. *International Journal of Remote Sensing* **26**: 2975–2993. DOI:10.1080/01431160500057798.

Kim M, Madden M, Warner T. 2008. Estimation of optimal image object size for the segmentation of forest stands with multispectral IKONOS imagery. In *Object-based image analysis, spatial concepts for knowledge-driven remote sensing applications*, Blaschke T, Lang S, Hay GJ (eds). Springer: Berlin; 291–307. DOI: 10.1007/978-3-540-77058-9_16.

Li YB, Shao JA, Yang H, Bai XY. 2009. The relations between land use and karst rocky desertification in a typical karst area, China. *Environmental Geology* **57**: 621–627. DOI: 10.1007/s00254-008-1331 -z.

Li YB, Wang SJ, Cheng AY, Li WH, Luo GJ. 2010. Assessment on spatial distribution of karst rocky desertification at different grid units. *Scientia Geographica Sinica* **30**: 98–102 (in Chinese with English abstract).

Liu YS, Wang J, Deng X. 2008. Rocky land desertification and its driving forces in the karst areas of rural Guangxi, Southwest China. *Journal of Mountain Science* **5**: 350–357. DOI: 10.1007/s11629-008 -0217-6.

Mitri G, Gitas I. 2004. A performance evaluation of a burned area object-based classification model when applied to topographically and non-topographically corrected TM imagery. *International Journal of Remote Sensing* **25**: 2863–2870. DOI:10.1080/01431160410001688321.

Muller E, Décamps H, Dobson MK. 1993. Contribution of space remote sensing to river studies. *Freshwater Biology* **29**: 301–312. DOI: 10.1111/j.1365-2427.1993.tb00766.x.

Myint SW, Gober P, Brazel A, Grossman-Clarke S, Weng Q. 2011. Per-pixel vs. object-based classification of urban land cover extraction using high spatial resolution imagery. *Remote Sensing of Environment* **115**: 1145–1161. DOI:10.1016/j.rse.2010.12.01.

Myint SW, Yuan M, Cerveny RS, Giri CP. 2008. Comparison of remote sensing image processing techniques to identify tornado damage areas from Landsat TM data. *Sensors* **8**: 1128–1156. DOI:10.3390/s8021128.

Neubert M, Herold H. 2008. Assessment of remote sensing image segmentation quality. *Proceedings GEOBIA 2008, Calgary, Canada.*

Neubert M, Herold H, Meinel G. 2008. Assessing image segmentation quality—concepts, methods and application. In *Object-based image analysis, spatial concepts for knowledge-driven remote sensing applications*, Blaschke T, Lang S, Hay G (eds). Springer: Berlin; 769–784. DOI: 10.1007/978-3-540-77058-9_42.

Stuckens J, Coppin PR, Bauer ME. 2000. Integrating contextual information with per-pixel classification for improved land cover classification. *Remote Sensing of Environment* **71**: 282–296.

Sweeting MM. 1995. *Karst in China*. Springer-Verlag: Berlin.

Tong LQ. 2003. A method for extracting remote sensing information from rocky desertification areas in Southwest China. *Remote Sensing for Land & Resource* **4**: 35–38 (in Chinese with English abstract).

Tormos T, Kosuth P, Durrieu S, Dupuy S, Villeneuve B, Wasson J. 2012. Object-based image analysis for operational fine-scale regional mapping of land cover within river corridors from multispectral imagery and thematic data. *International Journal of Remote Sensing* **33**: 4603–4633. DOI: 10.1080/01431161.2011.637093.

Van de Voorde T, De Genst W, Canters F. 2007. Improving pixel-based VHR land-cover classifications of urban areas with post-classification techniques. *Photogrammetric Engineering and Remote Sensing* **73**: 1017–1027.

Wang SJ. 2002. Concept and its connotation of karst rocky desertification. *Carsologica Sinica* **21**: 101–105 (in Chinese with English abstract).

Wang SJ, Liu QM, Zhang DF. 2004. Karst rocky desertification in southwestern China: geomorphology, landuse, impact and rehabilitation. *Land Degradation & Development* **15**: 115–121. DOI: 10.1002/ldr.592.

Wang XY. 2010. Comprehensive treatment of rocky desertification in karst mountain areas. *Chinese Journal of Agricultural Resources and Regional Planning* **31**: 76–80 (in Chinese with English abstract).

Whiteside TG, Boggs GS, Maier SW. 2011. Comparing object-based and pixel-based classifications for mapping savannas. *International Journal of Applied Earth Observation and Geoinformation* **13**: 884–893. DOI:10.1016/j.jag.2011.06.00.

Willhauck G, Schneider T, De Kok R, Ammer U. 2000. Comparison of object oriented classification techniques and standard image analysis for the use of change detection between SPOT multispectral satellite images and aerial photos. *Proceedings of XIX ISPRS*; 16–22.

Xia XQ, Tian QJ, Du FL. 2006. Retrieval of rock-desertification degree from multrspectral renote sensing images. *Journal of Remote Sensing* **10**: 469–474 (in Chinese with English abstract).

Xiong YJ, Qiu GY, Mo DK, Lin H, Sun H, Wang QX, Zhao SH, Yin J. 2008. Rocky desertification and its causes in karst areas: a case study in Yongshun County, Hunan Province, China. *Environmental Geology* **57**: 1481–1488. DOI: 10.1007/s00254-008-1425-7.

Yan G, Mas JF, Maathuis B, Xiangmin Z, Van Dijk P. 2006. Comparison of pixel-based and object-oriented image classification approaches—a case study in a coal fire area, Wuda, Inner Mongolia, China. *International Journal of Remote Sensing* **27**: 4039–4055. DOI:10.1080/01431160600702632.

Yan LH, Zhou ZF, Yu Q. 2009. An automatic classification model of karst rocky desertification based on neural networks combined with spectral-features—a case study of Shiqiao watershed of Yachi demonstration area in Bijie City of Guizhou Province. *Modern geographical sciences and Guizhou socio-economic* (in Chinese with English abstract). Guizhou Science & Technology Publishing Press: Guiyang.

Yu Q. 2009. *Research on the spectrum automatic extracting based on decision tree model of karst rocky desertification*. Guizhou Normal University: Guiyang (in Chinese with English abstract).

Yu Q, Gong P, Clinton N, Biging G, Kelly M, Schirokauer D. 2006. Object-based detailed vegetation classification with airborne high spatial resolution remote sensing imagery. *Photogrammetric Engineering and Remote Sensing* **72**: 799–811.

Yue YM, Wang KL, Zhang B, Jiao QJ, Yu YZ. 2008. Karst rocky desertification information extraction with EO-1 Hyperion data. *International Conference on Earth Observation Data Processing and Analysis (ICEODPA)*; 72854A.

Yue YM, Zhang B, Wang KL, Li R, Liu B, Zhang MY. 2011. Remote sensing of indicators for evaluating karst rocky desertification. *Journal of Remote Sensing* **15**: 722–736.

Zhang Y, Hu J, Xi H, Zhu Y, Chen DM. 2008. Analysis of rocky desertification monitoring using MODIS data in Western Guangxi, China. In *Advances in data, methods, models and their applications in geoscience*, Chen DM (ed). InTech: Rijeka, Croatia; 300–312.

Zhou ZF. 2001. Application of remote sensing and GIS technology for land desertification in Guizhou karst region. *Bulletin of Soil and Water Conservation* **21**: 52–54 (in Chinese with English abstract).